Building response to tunnelling- and excavation-induced ground movements: using transfer functions to review the limiting tensile strain method

Korhan Deniz Dalgic[a,b], Max A. N. Hendriks[b,c], Alper Ilki[a]

[a]*Civil Engineering, Faculty of Civil Engineering, Istanbul Technical University, Ayazaga Campus 34469 Istanbul, Turkey;* [b]*Structural Engineering, Faculty of Civil Engineering and Geosciences, Delft University of Technology, Stevinweg 1, 2628 CN Delft, The Netherlands;* [c]*Structural Engineering, Norwegian University of Science and Technology, Richard Birkelands vei 1A, 7491 Trondheim, Norway*

Corresponding author: Korhan Deniz Dalgic (dalgickorhandeniz@gmail.com)

Max A. N. Hendriks (M.A.N.Hendriks@tudelft.nl, max.hendriks@ntnu.no)

Alper Ilki (ailki@itu.edu.tr)

Building response to tunnelling- and excavation-induced ground movements: using transfer functions to review the limiting tensile strain method

In this paper, limiting tensile strain method (LTSM) is reviewed and advantages and disadvantages resulted from the simplicity of this method are examined in the light of the findings of the existing experimental and numerical studies. Using the viewpoint of the transfer functions for the LTSM, a more independent sight for the interpretation of the relationships between deflection ratio, structure's geometry, longitudinal/shear stiffness ratio and the limiting tensile strain is provided. In addition, the effect of average horizontal strain is included simply in the modified deep beam equations. Using reported data and observed damage classes of real and simulated case studies available in the literature, back-calculations for the coefficients of the transfer function are made. After comparing the back-calculated coefficients to the original coefficients of the LTSM, it is shown that observed damage and measured crack widths are reasonably compatible with the proposed limiting tensile strain boundaries. Also, it is shown that for the cases in which moderate or higher damage was observed, the original deep beam equations tend to underestimate the resultant damage.

Keywords: settlement; tunnels & tunnelling; excavation; damage assessment; brick masonry

1. Introduction

The building response to induced ground movements due to tunnelling or adjacent deep excavations has been of interest to an increasing number of researchers since the 1970s. The pioneering studies of Terzaghi (1935), Skempton and MacDonald (1956), Meyerhof (1956), Polshin and Tokar (1957) and Bjerrum (1963), which have particularly focused on building settlement due to building self-weight, have led to empirical-analytical approaches that are still in use for the prediction of building response to tunnelling- and excavation-induced ground movements. At this point, Burland and Wroth (1974) and Boscardin and Cording (1989) should be particularly mentioned, as they are responsible for two important developments: LTSM (Limiting Tensile Strain Method) and the inclusion of the effect of horizontal ground movements. They also proposed damage classifications that are still in use. Afterwards, significant improvements, such as the strain superposition method (Boone, 1996), the relative stiffness method (Potts & Addenbrooke, 1997) and the laminate beam method (Finno, Voss, Rossow, & Blackburn, 2005), were proposed. All these studies resolve issues resulting from the simplicity of the fictitious deep beam analogy adopted in the LTSM.

However the LTSM, owing to its simplicity, is still frequently used in the second-stage risk assessment of the buildings in many excavation projects. Moreover, final risk decision for the majority of the examined buildings is made in the second-stage assessment by using this method. Therefore the LTSM needs to be reviewed in detail and improved to increase the accuracy of the risk assessment procedure. On the other hand, limited number of studies (Son & Cording, 2007; Netzel, 2009) were devoted to review this method in detail.

In this paper, an overview for the LTSM is presented and the approaches adopted in this method are evaluated with the findings of experimental and numerical studies available in the literature. A different perspective, which will be called a transfer function view, is provided by re-formulating the original fictitious deep beam equations used in the LTSM.

3

Transfer functions offer a more independent sight for the interpretation of the relationships between deflection ratio, structure's geometry, longitudinal/shear stiffness ratio and the limiting tensile strain. Additionally, the horizontal strain can be involved directly into the deep beam equations. By means of back-calculated coefficients of the transfer functions from the 11 case studies and including the effects of horizontal strains, the compatibility between crack widths reported by Burland et al. (1977) and the limiting tensile strains suggested by Boscardin and Cording (1989) is examined.

2. Tunnelling- and excavation-induced ground movements and associated building deformation

2.1. Nature of the ground movements due to tunnelling and deep excavations

Tunnelling and deep excavations usually result in vertical and horizontal ground movements in their influence area. According to Boscardin (1980), the main causes of excavation-induced ground movements are an alternation in the state of stress within the ground, ground loss or soil removal, and change in the groundwater regime. In addition, the construction technique, excavation size, soil type and stiffness, stiffness of excavation support and support spacing, delayed support and grouting installation, and face stability (in tunnels) are other significant parameters affecting the magnitude of tunnelling- and excavation-induced ground movements (Son, 2003).

During a tunnel excavation, induced ground settlements form a trough shape perpendicular to the tunnel line (Figure 1(a)). If the ground surface is free of buildings, this shape is called the free-field ground settlement profile.

In addition, ongoing tunnel excavations can also result in advancing ground settlements in the longitudinal direction of the tunnel line. Furthermore, both in perpendicular and longitudinal direction, significant horizontal movements can occur.

In a tunnelling-induced ground settlement profile, while the concave part of the

profile is referred to as sagging, the convex part is referred to as hogging. Buildings can be situated in different positions with respect to tunnel line and they can modify ground settlements depending on their restraint capabilities (size, weight, foundation type, etc.) (Comodromos, Papadopoulou & Konstantinidis, 2014; Potts & Addenbrooke, 1997). In Figure 1 (a), different buildings that are sagging (i), in the vicinity of the inflection point (ii) and hogging (iii) are schematically illustrated (settlement modification is not shown in Figure 1(a)). In this figure, e refers to the eccentricity between the centre of the building and the tunnel centre.

Deep excavations are influential in a lateral distance ranging from two times to four times the excavation depth (Peck, 1969; Clough & O'Rourke, 1990). Several empirical and semi-empirical models have been proposed to predict the free-field ground settlement profile due to adjacent deep excavations (Peck, 1969; Clough & O'Rourke, 1990 and Hsieh & Ou, 1998). Hsieh and Ou (1998) introduced possible ground settlement profiles as shown in Fig 1 (b). The authors proposed two different methods to calculate spandrel and concave ground settlement profiles based on the estimated wall deformation.

[Figure 1 near here]

2.2. Building deformation measures

Tunnelling- and excavation-induced ground movements can damage surface buildings by impinging on their foundations. Building deformation measures note measurable geometrical distortions of buildings that are under the influence of tunnelling- and excavation-induced ground movements. They are used to establish correlations between geometrical distortions and building damages.

In Figure 2, building deformation measures that have commonly been adopted in the previous studies (differential settlement δS_v, angular distortion β and deflection ratio Δ/L) are schematically described considering the potential ground settlement modes (previously

5

shown in Figures 1(a)-(b)).

[Figure 2 near here]

As shown in Figures 2(a-c), as the ground settles due to a tunnelling or deep excavation, adjacent points A and B on the masonry wall perpendicular to the tunnelling line or excavation wall are displaced to points A' and B', resulting in straining within the wall. In this case, the differential settlement δS_v between points A and B is calculated using Equation (1). In this equation, $S_{v,A}$ and $S_{v,B}$ represent the vertical movement of points A and B, respectively. Uniform settlements ($S_{v,A} = S_{v,B}$) of buildings can also result in major serviceability problems related to building access and connection to utility lines.

$$\delta S_v = S_{v,A} - S_{v,B} \tag{1}$$

Apart from differential settlement, there are two other important damage measures that are frequently used in the literature: angular distortion (β) and deflection ratio (Δ/L). Skempton and MacDonald (1956) were first to introduce the angular distortion term as a damage measure for the investigation of settlement-induced damage. They defined it as the ratio between the differential settlement of two adjacent points on the structure and the distance between these points (between points A and B, it could be $\beta = \delta S_v/L$). Afterwards, Boscardin (1980) modified the definition of β such that the contribution of rigid rotation of the building (ω) (sometimes referred to as tilt) is excluded. It is known that ω corresponds to the free rotation of a building and does not cause any straining within the building (Figure 2(g)). In the current literature, β is calculated using the absolute-value expression in Equation (2) as modified by Boscardin. To calculate β, the other geometrical quantity required is the slope of the ground settlement profile (φ). ω and φ can be measured directly on the site or determined through the predicted site settlement contours. Note that the maximum value of β (β_{max}) should be considered. β_{max}, ω and φ are shown schematically on deformed building foundation lines in Figures 2(a-c).

$$\beta = |\omega - \varphi| \tag{2}$$

Polshin and Tokar (1957) proposed the deflection ratio (Δ/L), which is another important damage measure in the literature. Herein, Δ represents the maximum value of the vertical differential distance between the deflected foundation line and the straight line connecting points A and B (Figures 2(a-c)). Δ/L is then obtained by dividing Δ by the corresponding span length L. If the building spans the inflection point (Figure 1(a-ii)), it is possible to calculate Δ/L for both the sagging and hogging part of the wall. For these buildings, each part can be considered separately (Mair, Taylor, & Burland, 1996). Δ/L is represented as Δ_{sag}/L_{sag} for sagging and Δ_{hog}/L_{hog} for hogging. Herein, L_{sag} and L_{hog} represent the lengths of the building parts that are sagging or hogging, respectively.

Polshin and Tokar put forward some limitations for the Δ/L of buildings based on the site observations and building characteristics, such as building length to height ratio (L/H) (geometrical) and critical tensile strain (ε_{crit}) (on the material level). Note that the choice of L/H as an influential parameter is important because it practically corresponds to a measure of the building stiffness. On the other hand, ε_{crit} refers to tensile strain value attained at the onset of visible cracking in load-bearing masonry or infill walls of frame structures. Polshin and Tokar (1957) proposed 0.05% for ε_{crit} value for brick load-bearing masonry walls. A similar range (0.038 - 0.06%) was previously suggested by Burhouse (1969). This approach in which Δ/L, L/H and ε_{crit} were associated would later form the basis for the development of limiting tensile strain method (LTSM).

Some typical tunnelling- and excavation-induced building damages are shown with schematic illustrations in Figure 2(d-f). However, it should be reiterated that damage initialization and propagation are quite complicated and can be affected by numerous different parameters, such as L/H, shear/axial stiffness ratio of the brick-mortar interface in masonry buildings and soil-structure interaction. Furthermore, many researchers have

7

highlighted that cracking due to shear and bending usually occurs simultaneously in actual cases. Apart from these, buildings might tend to experience rigid rotation instead of serious distortion, especially in one or more of the cases where the settlement profile is wide enough, the L/H is high or the building has a very stiff mat foundation (Figure 2(g)). In these cases, limited damage can be expected due to horizontal strains.

3. Limiting tensile strain method (LTSM)

3.1. Fictitious deep beam analogy of Burland and Wroth (1974)

Burland and Wroth (1974) extended Polshin and Tokar's (1957) study and put forward a deep beam analogy for masonry and frame structures to calculate simply limiting tensile strain values (ε_{lim}). ε_{lim} is an useful parameter to detect bending or diagonal tensile cracking (shear) damages because it is independent of the loading direction and deflection mode (sagging or hogging). ε_{lim} can also be used under any loading circumstance.

The model of the fictitious deep beam which is assumed to be representative of real structures is given in Figure 3. The midpoint deflection (Δ) is considered to occur in either the hogging or sagging ground settlement zone. L denotes the length of the beam (in reality, it may correspond to the deflected or entire length of the structure), and H is the height of the beam. In reality, H corresponds to the building height from the foundation level up to the eaves. The roof is not included in the calculations. The fictitious deep beam is elastic, isotropic and simply supported. Soil-structure interaction is ignored and only free-field ground settlements are considered.

[Figure 3 near here]

The problem is solved by using the beam equation given in Equation (3). In this equation, E and G are assumed to indicate the elasticity and the shear modulus of the represented building (or a wall of a masonry building), respectively. However, they are always taken into account as a relative stiffness in the form of E/G alluding to structural

8

longitudinal/shear stiffness ratio. I is the second moment of the area of the fictitious deep beam. P corresponds to a central point load. This equation was previously developed by Timoshenko (1957) for central loaded and simply supported elastic beams considering the shear coefficient k=1.5. Note that this equation accounts for the combined contribution of bending and shear to the midpoint deflection.

$$\Delta = \frac{PL^3}{48EI}\left[1 + \frac{18EI}{L^2HG}\right] \tag{3}$$

Netzel (2009) proposed that the shear coefficient considered in this equation (k=1.5) should be updated with k=1.2 to prevent an overestimation of the shear deflection contribution.

If this equation is adapted to express the vertical settlement response of a building, P does not correspond to a true central load but instead refers to a factor revealing a deformation mode, as in the case of a real ground settlement. To justify the validity of the central loading in the representation of building deformation due to settlement, Burland and Wroth (1974) investigated the effect of two additional loading and deformation cases. These are a uniformly distributed loading case and a circular deflection mode. They observed that crack initialization is not sensitive to the use of these alternative loading and deflection mode applications. Therefore, it was suggested to use the central point loading P, which remarkably simplifies the calculations.

If Equation (3) is rewritten in terms of maximum bending tensile strain ε_{bmax} and Δ/L is isolated, Δ/L can be related to ε_{bmax} as shown in Equation (4). This equation applies to the case in which the first visible crack is assumed to arise in bending due to sagging or hogging of the structure. ε_{bmax} denotes the maximum tensile strain that occurs at the outermost fibre of the fictitious model beam once the induced Δ/L is completely achieved. In Equation (4), t represents the neutral axis depth from the edge of the beam in tension.

$$\frac{\Delta}{L} = \left[\frac{L}{12t} + \frac{3EI}{2tLHG}\right]\varepsilon_{bmax} \qquad (4)$$

Similarly, Equation (3) can be rewritten in terms of the maximum diagonal tensile strain ε_{dmax}. If Δ/L is isolated, Δ/L can be related to ε_{dmax} as shown in Equation (5). This equation applies to the case in which the first visible crack is assumed to arise in shear due to sagging or hogging of the structure. ε_{dmax} denotes the maximum tensile strain that occurs in the diagonal direction once the induced Δ/L is completely achieved.

$$\frac{\Delta}{L} = \left[1 + \frac{HL^2G}{18EI}\right]\varepsilon_{dmax} \qquad (5)$$

Equations (4) and (5) are particularly derived to establish separate expressions between Δ/L and the maximum tensile strains (ε_{bmax} and ε_{dmax}) that might be responsible for potential tensile cracking in either bending or shear. Note that ε_{bmax} and ε_{dmax} are not necessarily critical tensile strain (ε_{crit}) at this stage. To determine a damage level, the calculated maximum tensile strains (ε_{bmax} or ε_{dmax}, whichever is greater) is compared to predefined limiting tensile strain boundaries ($\varepsilon_{lim(low)}$ and $\varepsilon_{lim(up)}$) listed in Table 1 proposed by Burland et al. (1977) and modified by Boscardin and Cording (1989).

3.2. Combining the maximum tensile strain with horizontal strain (Boscardin and Cording, 1989)

Ground movements induced by excavations, such as tunnelling, open-cut and mining, involve significant horizontal displacement components. Boscardin and Cording (1989) reported that, horizontal strains transferred from the ground to the structure can remarkably decrease the settlement tolerances of buildings together with bending and diagonal tensile strains. Since the fictitious deep beam approach by Burland and Wroth (1974) does not include the effect of horizontal strain, Boscardin and Cording considered this effect by combining the average horizontal strain (ε_h) with ε_{bmax} and ε_{dmax} values.

Horizontal strain is assumed to be equally distributed over the height of the structure. In reality, horizontal strains are much higher in the lower parts of structures that are close to the foundation (Son and Cording, 2005). While $S_{h,A}$ and $S_{h,B}$ are the monitored horizontal movements at A and B sections of a wall, ε_h can be calculated as shown in Equation (6). ΔS_h denotes the differential horizontal movement (Equation (7)) and L shows the initial distance between these two sections. For structures with individual footings (frame structures), differential horizontal movement between adjacent footings is taken into account to calculate average horizontal strains. If there is no other information such as monitoring results, Boscardin and Cording (1989) suggested that ε_h value acted on a brick wall can be assumed as 0.5 to 1 times the change in the slope of the free-field ground settlement profile for braced excavations and tunnelling and 1 to 1.5 times the change in slope of the free-field ground settlement profile for excavations with cantilever walls. It has to be highlighted that this assumption can be valid as long as there is no tensile reinforcement in the footings or in the walls.

$$\varepsilon_h = \frac{\Delta S_h}{L} \tag{6}$$

$$\Delta S_h = S_{h,A} - S_{h,B} \tag{7}$$

The combined tensile strain, namely the total tensile strain (ε_t), is then calculated as shown in Equations (8) and (9). While ε_{bmax} and ε_h are easily summed (Equation (8)), ε_{dmax} and ε_h are combined by using Mohr's Circle (Equation (9)). The result of Equation (8) or Equation (9), whichever is greater, is taken and compared with the limiting tensile strain boundaries listed in Table 1 to determine the corresponding final damage class.

If β is selected as the deformation measure instead of Δ/L (it is thought that damage is to be governed by the combined effect of shear and horizontal strain), a different combination proposed by Son and Cording (2005) can be used. According to Son and

Cording, for given values of β and ε_h, total tensile strain ε_t in a part of structure can be derived in a similar manner of calculating principal tensile strain ε_p. ε_t (equal to ε_p) is calculated using Equation (10), where θ_{max} is the crack orientation measured as the angle between the plane on which ε_t acts and the vertical plane. After comparing the calculated ε_t with the limiting tensile strains boundaries listed in Table 1, the damage class is determined.

$$\varepsilon_t = \varepsilon_{bmax} + \varepsilon_h \tag{8}$$

$$\varepsilon_t = \frac{\varepsilon_h}{2} + \sqrt{\left(\frac{\varepsilon_h}{2}\right)^2 + \varepsilon_{dmax}{}^2} \tag{9}$$

$$\varepsilon_t = \varepsilon_p = \varepsilon_h \cos\theta_{max}^2 + \beta \sin\theta_{max} \cos\theta_{max} \tag{10}$$

$$\tan(2\theta_{max}) = \frac{\beta}{\varepsilon_h} \tag{11}$$

[Table 1 near here]

The presence of RC mat foundations or strip foundations connected by continuous slabs provides a significant tensile restraint. Consequently, horizontal ground movements are substantially reduced or inhibited at the foundation level (Boscardin & Cording, 1989; Burland, Mair, & Standing, 2004; Son & Cording, 2007). On the other hand, the presence of foundation piles in the proximity of an excavation can reduce the horizontal ground movements (Basile, 2014; Mroueh & Shahrour, 2002).

The effect of RC continuous and individual footings of frame structures was numerically investigated by Goh and Mair (2014). They found that, while horizontal strains are usually insignificant for frame structures with continuous footings, they are important for frames with individual footings even when the axial stiffness of the frame building is high. This result is in line with the findings of Laefer et al. (2009) in which scaled RC frame specimens with individual column footings were tested and numerically simulated. Laefer et

al. observed a significant increase in the drift ratio of especially the first storeys of frame structures when the horizontal ground movements are included.

3.3. Damage classification and practical design charts

As aforementioned, damage class is decided by comparing calculated maximum total tensile strain to predefined limiting tensile strain boundaries ($\varepsilon_{lim(low)}$, $\varepsilon_{lim(up)}$) presented in Table 1. Note that this table was priorly proposed by Burland et al. (1977) and modified after Boscardin and Cording (1989) by adding $\varepsilon_{lim(low)}$ and $\varepsilon_{lim(up)}$ boundaries. As shown, defined damage categories are essentially based on ease of damage repair. Therefore, this classification applies mostly to load-bearing masonry walls (brick & stone). However, there are cases in which it was used for infill walls of frame structures (as in the case study of the RC Elizabeth House building by Mair & Taylor, 2001). The authors of the current paper think that these damage categories also require verification for different masonry wall typologies having different construction techniques (i.e., multi-leaf walls). Burland et al. (1977) noted that crack widths in this classification are to be used as an additional indicator rather than being a direct measure of damage. They also highlighted that damage is usually difficult to quantify because it depends on many subjective criteria. On the other hand, damage that is acceptable in a region or for one type of building might not be acceptable for other cases. Therefore, although this damage classification is widely used, users should keep in mind that it reflects generalized cases.

For the practical use of the LTSM, some diagrams based on the damage classifications given in Table 1 were proposed by Boscardin and Cording (1989) and Burland (1997) (Figure 4).

[Figure 4 near here]

As shown in Figure 4(a), the diagram proposed by Boscardin and Cording (1989) shows the limiting curves that are boundaries of different damage classes predefined in Table 1. To obtain these curves, fictitious deep beam (with $L/H = 1$ and $E/G = 2.6$) equations derived for hogging ($t = H$) are used together with the given limiting tensile strain boundaries $\varepsilon_{lim(low)}$ and $\varepsilon_{lim(up)}$. In order to obtain presented β values in this diagram (β_{max} at the support sections of centrally loaded deformed fictitious deep beam), Equation (12) is used. For typical values of L/H and E/G, this expression gives β_{max} values that vary between 2 or 2.3 times Δ/L.

$$\beta_{max} = \frac{3\Delta}{L}\left[\frac{1 + 4\left(\frac{E}{G}\right)\left(\frac{H^2}{L^2}\right)}{1 + 6\left(\frac{E}{G}\right)\left(\frac{H^2}{L^2}\right)}\right] \tag{12}$$

A limited amount of case study data are also provided to validate the damage categories. The case study data consists of infilled steel frame, infilled wood frame and brick masonry structures that are mostly small to medium in size. Boscardin and Cording reported that none of these structures was capable of modifying the free-field ground movements due to their relatively small/medium size and absence of a grade beam.

The other diagram proposed by Burland provides a similar interaction between ε_h and Δ/L (Figure 4(b)). By combining Equations (4) & (5) with (8) & (9) respectively, and setting $\varepsilon_{bmax} = \varepsilon_{lim}$ or $\varepsilon_{dmax} = \varepsilon_{lim}$, the curves given in Figure 4(b) are obtained for each damage class given in Table 1. Note that for the derivation of these curves the hogging condition is considered ($t = H$) along with $L/H = 1$ and $E/G = 2.6$. As seen, for a given Δ/L, as the acted horizontal strain increases, the damage class shifts from lower to higher damage. Burland criticises Boscardin and Cording's diagram as to that maximum bending strains ε_{bmax} are ignored. This criticism can be seen as an extension of another discussion where the fact that the use of beta is mostly being related to shear behaviour of the structure was

asserted. In addition, Burland states that Equation (12) used by Boscarding and Cording to calculate β_{max} from Δ/L is very sensitive to the load distribution.

3.4. Reported deficiencies of the LTSM

To determine the ultimate risk level of the buildings subjected to tunnelling-induced ground movements, a three-staged process is conducted: preliminary assessment, second-stage assessment and detailed assessment (Mair et al., 1996). LTSM is a widely accepted practical tool for second-stage assessment of, in particular, brick masonry walls affected by tunnelling-induced ground movements. Because the final risk decision for the majority of investigated buildings is to be made in the second-stage assessment, the accuracy of the LTSM is important. For instance, during the tunnel and shaft excavations of Sirkeci Underground Station of the Marmaray Project in Turkey, 135 buildings were examined in the second-stage assessment (after a preliminary assessment), and 58 of these buildings (40%) (with moderate and high risk) were re-assessed in the detailed assessment stage. In other words, for 60% of these structures, the final risk decision was made according to the results of the second-stage assessment. This situation indicates the importance of the second-stage assessments. If the accuracy and precision of the LTSM is increased, it not only enhances the accuracy of final risk decisions but also may reduce the number of buildings that are to be assessed by expensive and time-consuming methods such as finite element methods in the detailed assessment stage.

However, due to its simplistic nature, use of the LTSM cannot be sufficient. The most frequently reported deficiencies of the LTSM are presented below. These shortcomings have stimulated other methods and approaches.

(1) Structural differences and variety (at both the structural and material levels) cannot be sufficiently reflected. Simply using different fictitious values for E/G does not guarantee that different structures with different structural systems, compositions,

materials, irregularities, etc., are represented well. When the detailed stress, strain and damage distributions are important, as in the case of frame structures, LTSM and conventional deformation measures cannot be sufficient (Laefer et al., 2009). In these cases, finite element analyses can be crucial.

(2) The effect of different types of foundations cannot be considered. Assumptions made for the position of the neutral axis might not reflect actual cases if the structural system is complicated.

(3) Only one type of settlement deflection mode is considered, and the validity of this deflection mode (a deflected shape of a simply supported beam under a central load) is limited by the building length L. If the building length is too long or short, the simply supported beam approach becomes invalid (Boone, 1996; Finno et al. 2005).

(4) In calculations, free-field ground movements are used. Moreover, these are directly imposed on the fictitious model beam assuming there is no relative movement between building and soil. The soil-structure interaction is ignored. This assumption generally results in more conservative estimates of the building response. However, in reality, there is a dual interaction between soil and structures (Boscardin & Cording, 1989; Murphy, Gaynor and Laefer, 2010; Potts & Addenbrooke, 1997).

(5) Although recent works (Clarke & Laefer, 2014) have started suggesting an index-based approach to incorporate the existing condition of buildings into building risk assessment framework, initial damage to the buildings (existing cracks, etc.) is not originally accounted for in the LTSM. This may lead to overestimation of the initial stiffness. Furthermore, widening of the existing cracks and damage accumulation during ground settlement cannot be considered. This situation might lead to un-conservative damage predictions. Fok, Neo, Goh and Wen (2012) suggested that

detailed assessments should always be conducted for buildings that are found to be in poor conditions in preliminary assessment.

(6) Nonlinearity of building materials and stiffness degradation during settlements cannot be considered. On the contrary, the finite element analyses and laboratory tests performed by Son and Cording (2005), Laefer et al. (2009) and Giardina et al. (2012) showed that consideration of nonlinear material properties (cracking) has a significant influence on masonry wall and frame stiffness and thus overall response.

(7) The effect of tunnelling activities parallel to the tunnel axis is ignored. Therefore, the potential torsional response of buildings underground movements cannot be considered. Furthermore, because a plane stress condition is considered, the contributions of the other walls and slabs that are orthogonal to the considered plane are not taken into account (Giardina, 2013).

(8) Building self-weight is ignored. On the contrary, there are several reported results in the literature that highlight the effect of building self-weight (Boonpichetvong M, Netzel H, & Rots, 2006; Burd, Houlsby, Augarde, & Liu, 2000; Fargnoli, Gragnano, Boldini, & Amorosi, 2015; Franzius, Potts, & Burland, 2006; Giardina, DeJong, & Mair, 2015b; Mroueh & Shahrour, 2003; Laefer et al., 2009). In general, it is understood that the conformity to the ground settlement profile is increased by increased building self-weight. Thus, larger distortions and internal forces arise. In addition, redistribution of the building self-weight during on-going excavations can result in a partial embedment of the structure into the soil (Farrell, Mair, Sciotti & Pigorini, 2014).

4. Viewing the LTSM as transfer functions

In section 3, the basic idea behind the LTSM is presented. In this section, Equations (4) and (5) based on the fictitious deep beam analogy are presented as transfer functions. Thus, a new perspective is provided for easier and more independent interpretation of the relationships between deflection ratio (Δ/L), structure's geometry (L/H), stiffness ratio (E/G) and tensile strains.

Setting the ε_{bmax} and ε_{dmax} values in Equations (4) and (5) as ε_{crit}, these equations can be re-formulated as transfer functions such as $\Delta/L = C\varepsilon_{crit}$. Herein, C corresponds to coefficients in Equations (4) and (5) that are dependent on the geometrical and stiffness properties L, H, E, G, I and t.

[Table 2 near here]

Table 2 shows extracted C coefficients calculated for sagging and hogging. While C_b is for the bending critical case, C_d is for the shear critical case. For sagging buildings, the neutral axis is assumed at the middle of the fictitious deep beam (Burland and Wroth, 1974). Hence, the neutral axis depth becomes $t = H/2$ in the calculations. The second moment of the area is calculated as $I = 1 \times H^3/12$ assuming a unit width of the beam. For buildings in hogging or if significant restraints (such as RC mat foundations) exist, the neutral axis is assumed to be along the bottom edge of the fictitious beam (Burland & Wroth, 1974). In this case, the neutral axis depth shifts from $t = H/2$ to $t = H$. I is calculated according to the new location of the neutral axis as $H^3/3$. The selected positions of neutral axis in sagging and hogging depend on the empirical observations made by Burland and Wroth. According to the authors, due to the presence of compression strains which are transferred from soil to the lower parts of the buildings in sagging, it can be assumed that the neutral axis positions at the centre line of the 'beam'. On the other hand, the buildings with especially shallow weak foundations are largely influenced by the tensile strains transferred from the soil in a hogging

zone. Burland and Wroth assumed that neutral axis should be at the bottom edge of the 'beam' to represent the vulnerability of these buildings. In other words, it is assumed that building walls work for tension. Boscardin and Cording (1989), Mair et al. (1996) and Son and Cording (2007) also support this assumption. The results of the numerical study by Son and Cording (2007) in which the response of a masonry model wall situated in the hogging zone is examined are in good agreement with the analytical results obtained using a fictitious cantilever deep beam model with the neutral axis along the bottom edge. According to Netzel (2009), if horizontal strains are not considered in damage calculation, the assumption of neutral axis is at the bottom edge leads to lower strains (compared to the case of neutral axis is at the centre line) in L/H range between 0.75 and 2.5. The author states that this situation is not in line with the main intention that was to increase the susceptibility of hogging buildings under only vertical ground movements.

4.1. *The effect of the E/G ratio in LTSM shown by transfer functions*

Burland and Wroth (1974) used three different E/G ratios (0.5, 2.6 and 12.5) to identify different structure types (masonry and frame structures) and to consider unique features of masonry structures such as window or door openings in load-bearing walls. According to elasticity theory, E/G equals $2(1 + v)$ for isotropic materials. For $v = 0.3$, E/G becomes 2.6. Burland and Wroth (1974) proposed $E/G = 2.6$ for massive load bearing walls (excluding openings) even if the massive masonry is not an isotropic and linear elastic material. They proposed $E/G = 12.5$ for buildings that are more flexible, such as RC open frames, so that they can conform to the settled ground profile more easily than infilled RC frames and rigid masonry wall structures. The aim of selecting a higher E/G value for these flexible structures was to consider their decreasing vulnerability in bending. For buildings with extremely high stiffness in shear (or little longitudinal stiffness), such as wall structures made of precast concrete units, $E/G = 0.5$ was proposed for hogging. Note that proposed

values were supported by only experiences of the authors without any other evidence. Furthermore these generalized values can significantly change from one building to another. Potts and Addenbrooke (1997) and Finno et al. (2005) proposed more realistic techniques to calculate the overall equivalent relative stiffness of masonry load-bearing and frame structures.

Many other researchers also empirically investigated the most reasonable values of E/G in different cases. Cook (1994) made back-calculations by modelling real masonry façade walls as fictitious deep beams. The author reported that E/G was taken as 30 in fictitious deep beam calculations to provide similar distortions with the actual façade walls. This value is remarkably higher than the values proposed by Burland and Wroth (1974). This was probably because the façade walls examined by Cook experienced mostly shear-related damages.

Son and Cording (2007) performed numerical tests to find equivalent normal and shear stiffness values for modelling masonry buildings subjected to settlement effects. They also investigated the effect of different opening ratios and brick-mortar interface properties on these equivalent stiffness values. Their findings supported the assumption that an increase in the opening ratio and/or a decrease of the shear/normal stiffness ratio of the brick-mortar interface results in dramatic increases of E/G. For a typical opening ratio and a typical range of the shear/normal stiffness ratio, an equivalent E/G of 12 was proposed.

Giardina, Hendriks, & Rots (2015a) performed sensitivity analysis using finite element modelling. They investigated the effects of many factors, including the opening ratio (0, 10 and 30%) and material parameters (elasticity modulus, tensile strength and fracture energy). After an extrapolation, they showed that E/G ratios of 2.6, 8 and 11 in the LTSM correspond to opening ratios of 0, 10 and 30% in their finite element model of masonry walls, respectively.

To visualize the effect of E/G, C coefficient versus L/H relationships can be used. The composite curves in Figures 5(a) and 5(b) show the minimum (and thus decisive) values of C_b and C_d as a function of L/H. Each curve is obtained for a different E/G value (12.5, 2.6, 4.0 and 0.5). While the composite curves given in Figure 5(a) are derived for sagging ($t = H/2$), those given in Figure 5(b) are derived for hogging ($t = H$).

Recalling the formulation of the transfer function, an increase in C coefficients results in a decrease in ε_{crit} values for a given Δ/L. Although ε_{crit} was introduced as a certain material property associated with the onset of cracking, herein, reduction in ε_{crit} corresponds to a decrease in cracking vulnerability. As shown in Figures 5(a) and 5(b), cracking is governed by shear for a lower range of L/H values for all values of E/G. As mentioned before, L denotes the affected length of the structure. It is not always necessarily the entire length of the structure. In the initial stages of a tunnelling or excavation, buildings act as if they have a low L/H. Boscardin and Cording (1989) and Son and Cording (2007) explained this fact by highlighting the propagating nature of tunnelling- and excavation-induced ground movements. According to them, ground movements usually proceed over time, and L, impinged by the ground movements, increases progressively. The figure thus illustrates that, in the initial stages of a tunnelling or excavation (for lower values of L/H), diagonal cracks (as an indicator of the shear dominating response) in the walls are more likely to occur.

Another interesting point that was underlined by Burland and Wroth (1974) concerns the range of L/H that induces shear in sagging and hogging. As shown, for buildings in hogging, this range is twice the corresponding range for sagging for all E/G ratios. The dominating coefficient is altered from shear to bending at different values of L/H depending on the value of E/G. As the longitudinal stiffness is increased (or the shear stiffness is decreased), the range of L/H with dominating shear damage is extended in both sagging and hogging (Figures 5(a) and 5(b)). This result is in line with the notion that, if E/G increases,

the range of L/H where shear is responsible for crack initialization is extended. For buildings with a low E/G of 0.5, almost the entire range of L/H is dominated by bending in both sagging and hogging (Figures 5(a) and 5(b)).

[Figure 5 near here]

4.2. Implementation of horizontal strains in the transfer function of LTSM

The effect of horizontal strains can be introduced to the transfer function concept for the hogging cases. To achieve this, transfer function equation is re-expressed in terms of the total tensile strain ε_t and the horizontal strain ε_h, as shown in Equations (13) and (14). For this purpose, ε_{bmax} and ε_{dmax} are isolated in Equations (8) and (9) and then expressed as $(\varepsilon_t - \varepsilon_h)$ and $(\varepsilon_t - \varepsilon_h \cos 45)$, respectively. During the isolation of ε_{dmax} from Equation (9), the diagonal component of ε_h can be simply taken as $\varepsilon_h \cos 45$ assuming that it is in the 45° inclined plane with respect to the horizontal direction. If each side of Equations (13) and (14) is linearized in ε_t, the expressions can be rewritten as shown in Equations (15) and (16). Herein, the adapted coefficients $C_b{}^*$ and $C_d{}^*$ are functions of C_b, C_d and the $\varepsilon_h/\varepsilon_t$ ratio.

$$\Delta/L = C_b \varepsilon_{bmax} = C_b(\varepsilon_t - \varepsilon_h) \tag{13}$$

$$\Delta/L = C_d \varepsilon_{dmax} = C_d \sqrt{\varepsilon_t{}^2 - \varepsilon_t \varepsilon_h} \cong C_d(\varepsilon_t - \varepsilon_h \cos 45) \tag{14}$$

$$\Delta/L = \left[C_b \left(1 - \frac{\varepsilon_h}{\varepsilon_t (= 0.0006)} \right) \right] \varepsilon_t = [C_b^*] \varepsilon_t \tag{15}$$

$$\Delta/L = \left[C_d \left(1 - \frac{\varepsilon_h}{\varepsilon_t (= 0.0006)} \cos 45 \right) \right] \varepsilon_t = [C_d^*] \varepsilon_t \tag{16}$$

Total tensile strain ε_t in $\varepsilon_h/\varepsilon_t$ can be assumed as critical tensile strain of brick masonry wall at the onset of visible cracking. Herein, ε_{crit} is taken as 0.06% complying with the suggestion of Burhouse (1969). Thus $\varepsilon_h/0.0006$ can be assumed as relative magnitude of average horizontal strain acted on the structure in hogging. If average ε_h value on the structure is known, $\varepsilon_h/0.0006$ ratio can be calculated. However, in many practical cases, it is

very difficult to measure the horizontal strains acted on the structures directly. Also they cannot be separated from the bending related lateral strains. In the cases in which ground movements are assumed to be transferred to the structure without any significant modification, building horizontal strains can be estimated by deriving the free-field ground settlement profile over the pertinent portion of the building. Horizontal strains can then be assumed as 0.5 to 1 times the change in the slope of the free-field ground settlement profile (Boscardin and Cording, 1989). Herein, it has to be noted that the results will be conservative.

For the known values of Δ/L, C_b and C_d and the estimated/measured value of $\varepsilon_h/0.0006$, a new value of ε_t is calculated through Equations (15) and (16). The corresponding damage class is then determined according to the new value of ε_t. In bending critical cases where the estimated/measured ε_h exceeds the $\varepsilon_{crit} = 0.06\%$ ($\varepsilon_h/\varepsilon_t \geq 1$) and in diagonal tensile strain critical cases where $\varepsilon_h > 0.085\%$, the damage class can be approximately determined by comparing ε_h directly to limiting tensile strain boundaries in Table 1. In other words, horizontal strain in those cases is assumed to be directly responsible for the prospective building damage. In Figure 6, the variation of $C_b{}^*$ and $C_d{}^*$ coefficients for varying L/H values is illustrated. Note that these curves are derived for a masonry wall with $E/G = 2.6$ situated in hogging. As shown, as $\varepsilon_h/\varepsilon_t$ increases (role of ε_h on prospective damage increases), the values of $C_b{}^*$ and $C_d{}^*$ are reduced. The reduction of $C_b{}^*$ is higher than that of $C_d{}^*$ because ε_h is working in parallel to the longitudinal strains due to bending. In addition, it should be noted that, as $\varepsilon_h/\varepsilon_t$ increases, bending critical range of L/H slightly increases because tensile strains in the longitudinal direction (due to bending and imposed horizontal strain) are increased. Note that a reduction of $C_b{}^*$ and $C_d{}^*$ results in an increase of the calculated new ε_t value and accordingly damage class for a given Δ/L.

[Figure 6 near here]

It is emphasized that the mentioned modifications to incorporate the effect of horizontal strains are performed basically for making evaluations for deep beam equations, as will be presented in the next subsection. The proposed modifications are not intended to constitute a new in-situ assessment methodology.

4.3. Back-calculation of the coefficients of the LTSM transfer functions from real and simulated case studies

Using the back-calculated coefficients of transfer functions and utilizing the implementation of the effect of horizontal strain, a simple evaluation of available data is conducted here (Table 3). For this purpose, the real case studies of Boscardin and Cording (1989) (case 1) and Farrell et al. (2014) (cases 7 and 8), the experimental data of Son (2003) (case 2) and Giardina et al. (2012) (cases 3-6) and numerical test data of Giardina et al. (2014) (cases 9-11) are used (Table 3). The specific intervals for C coefficients are then back-calculated to compare with C coefficients derived by the extracted deep beam equations in Table 2. Case 1 is a four-storey brick bearing wall structure subjected to ground movements due to the excavation of a twin tunnel. The foundation consists of rubble strip footings. An extensive shear damage was observed in the hogging part of one of the walls over a length which is almost equal to the wall height ($L/H\approx1$). Cases 7 and 8 refer to a two-storey brick bearing wall structure overlying a tunnel excavation. It also has strip footings. It was reported that this building responded relatively flexible to tunnelling-induced ground movements. Moderate level of damage was observed in the sagging and hogging parts of the building. Due to the complex nature of real site problems and lack of data reported, very few real case studies were available to make back-calculations. On the other hand, as being in a controlled environment, the measurements and results of laboratory tests and numerical tests offer advantages for the theoretical robustness of the back-calculation work. The cases 2-6 are therefore derived from experimental studies (Son, 2003 and Giardina et al., 2012) including

24

physical tests of a 1/10-scaled brick masonry façade with openings under artificial hogging conditions. Shear-related damages were observed for these cases. Note that the cases 3-6 are sub-steps of the wall experiment of Giardina et al. (2012). The last three cases (9-11) are the simulations created using the proposed damage functions of Giardina et al. (2014) in which many parametric nonlinear finite element analyses were conducted. All simulated cases include a brick masonry wall model which is similar in size to the wall physically tested in Giardina et al. (2012). The parametric damage functions allow the application of different opening ratios, different magnitude of Δ/L and sagging conditions.

[Table 3 near here]

Table 3 also lists the structural properties and deformation measures for each case, as well as the observed damage classes. The E/G column shows the values which are explicitly reported (for cases 3-6), extrapolated (for cases 2 and 9-11) and assumed (for cases 1, 7 and 8). A similar extrapolation technique (based on the suggestions of Son & Cording, 2007 and Giardina et al. 2015a) that is used for the cases 2 and 9-11 cannot be done for the cases 1, 7 and 8, due to missing information regarding the geometrical properties and opening ratios of the walls. However a small sensitivity study is conducted using different E/G values in the back-calculation process of these cases. In Table 3, $(\Delta/L)_{meas}$ represents either the ultimate deflection ratio for the cases 1, 2, 7, 8, 9, 10 and 11 or the deflection ratios attained at the end of various sub-steps in the experiment of Giardina et al., 2012 (cases 3-6). Note that Δ/L and the corresponding damage increased progressively during this experiment.

The effect of horizontal strains is also considered for the hogging cases 1, 2 and 8. While the horizontal strains in the cases 1, 7 (sagging) and 8 are calculated with the practical assumption that they vary between 0.5 and 1 times the change in the slope of the free-field ground settlement profile, in case 2 it was directly measured on the specimen wall. In the cases 3-6, no horizontal strain was considered by the authors due to the use of a lubricated

rubber interface between the test wall and supporting steel profile. Likewise, in the cases 9-11, horizontal strains are assumed to be zero because of the presence of a smooth interface at the wall base in the numerical analyses.

Damage classes were either explicitly reported based on the visual inspection results (cases 1, 7 and 8) or defined based on the maximum crack width and crack intensity (cases 2-6). For the cases 9-11, damage classes are directly defined as a result of the damage functions. Note that the maximum crack widths listed for the cases 2-6 are ten times the experimentally observed values to be in line with the field scale (Son, 2003 and Giardina et al., 2012).

Based on the reported data and damage classes, the evaluation procedure is performed as follows:

- C_b and C_d coefficients of the transfer function are calculated based on reported L/H and E/G values through the extracted original deep beam equations given in Table 2. The minimum of C_b or C_d is decisive on the dominant damage type (bending cracking or diagonal tensile cracking). The defined damage type is compared to observed damage type. For all of the cases presented here, the defined damage type is in line with the observed damage type.

- The range of $C_{(low)}$ and $C_{(up)}$ is back-calculated using Equations (17) and (18) substituting $(\Delta/L)_{\text{meas}}$ and $\varepsilon_{lim(low)}$ and $\varepsilon_{lim(up)}$ boundaries which correspond to the reported damage class. Note that back-calculation is based on only measured and observed case information and thus independent of the deep beam equations.

- The obtained back-calculated range $C_{(low)}$- $C_{(up)}$ is then compared to calculated C_b or C_d value, whichever is critical (minimum). In the hogging

cases, if exists, the effect of horizontal strain can also be considered. Note that incorporation of the horizontal strain will result in a reduction in the coefficients of the transfer functions (see Equations (15) and (16)).

$$C_{(low)} = \frac{(\Delta/L)_{meas}}{\varepsilon_{lim(up)}} \qquad (17)$$

$$C_{(up)} = \frac{(\Delta/L)_{meas}}{\varepsilon_{lim(low)}} \qquad (18)$$

4.4. Discussion of the results of performed back-analysis

This section presents and discusses the results obtained through the back-calculation of the C coefficients from the 11 case studies. Note that the aim of this back-calculation is not to make a verification of the current LTSM, but to provide a different perspective for future examinations. It should be noted that the crack widths given in Table 1 were not intended to be used on their own to decide on the damage class, which has been done here in the back-calculations. However, the results of the back-calculations are meant to show to what extent the observed damage and measured crack widths are compatible with the limiting tensile strain boundaries $\varepsilon_{lim(low)}$ and $\varepsilon_{lim(up)}$ introduced in the current damage classification method.

[Figure 7 near here]

Figure 7 compares the calculated C_b and C_d coefficients to back-calculated $C_{(low)}$-$C_{(up)}$ ranges for each case presented in Table 3. It should be stated that, for an ideal agreement between observed damage & measured crack widths and attributed limiting tensile strain boundaries, the calculated C_b and C_d coefficients are expected to locate in-between the back-calculated $C_{(low)}$ and $C_{(up)}$ boundary values. From this aspect, a general agreement between calculated C_b and C_d coefficients and back-calculated ranges is seen for the majority

of the examined cases. For the cases 2, 5, 8 and 11 in which moderate or higher damage was observed, the calculated decisive C_d coefficients tend to clearly overestimate the back-calculated C ranges. This might be because calculated C_d is a constant value and it cannot capture degraded stiffness beyond moderate damage of these structures. On the contrary, in the cases 3 and 9 in which negligible or slight damage was observed, the calculated decisive C_d coefficients tend to clearly underestimate the back-calculated C ranges. This might be because these structures response actually in a stiffer manner than being estimated by the deep beam approach.

Recalling the generic form of the transfer functions, $\Delta/L = C\varepsilon_{crit}$, it can be stated that overestimation of C_b or C_d will yield an underestimation of the damage for the structures having moderate or higher damage in reality. This situation can also be considered in the assessment procedure of the structures which are damaged prior to excavation works. However, being quite conservative as a result from the direct application of free-field ground settlements, the mentioned underestimation is most probably compensated during the evaluations made by LTSM.

For the cases 1, 4 and 6, in which moderate to very severe damage was observed, the calculated decisive C_d values tend to approach to the upper boundary of the back-calculated C ranges. In the cases 7 and 10, in which moderate damage was observed, the decisive C_b (for case 7) and decisive C_d (for case 10) tend to approach the lower boundary of the back-calculated C ranges. Note that case 7 corresponds to a bending critical case and thus C_b is decisive.

It has to be highlighted that the varying E/G values from 2.6 to 10 for the cases 1 and 8 has insignificant effect on the results of the evaluations made above. This is because the influence of the value of E/G on the determination of the decisive C_d coefficient is quite limited, especially for the hogging cases up to $L/H=2$ (see Figure 5(b)). Note that the

decisive C coefficient shifts from C_b to C_d for the values of $E/G \geq 11$ for case 7. This situation could have an effect on the evaluation of case 8.

There are only three cases (1, 2 and 8) for which the effect of horizontal strain can be incorporated. For the cases 1 and 2 the magnitude of the average horizontal strain ε_h exceeds 0.085%. Therefore, Equation (16) cannot be used. However, it is obvious that calculated C_d value would be lower for these cases. The arrows facing downward represent this expected reduction in the calculated C_d value (Figure (7)). Interestingly, the damage class of these two cases (severe for case 1 and moderate for case 2) can be determined by means of a direct comparison of the average horizontal strain to the limiting tensile strain boundaries $\varepsilon_{lim(low)}$ and $\varepsilon_{lim(up)}$. This situation might show that damage in these cases is governed by mainly horizontal strains. For case 8, in which average horizontal strain $\varepsilon_h < 0.085\%$, the overestimating C_d value (1.01) can be reduced to a C_d^* value (0.38) by using Equation (16). As seen in Figure (7), the reduced C_d^* value provides a better approximation to the back-calculated range.

5. Conclusions

In this paper, an overview for the LTSM is presented and the approaches adopted in this method are evaluated with the findings of existing studies available in the literature. A transfer function view of the fictitious deep beam equations is provided to offer a more independent sight for the interpretation of the relationships between deflection ratio, structure's geometry, longitudinal/shear stiffness ratio and the limiting tensile strain. The conclusions are presented as follows:

- LTSM as a practical tool is useful in the preliminary assessment stages of the buildings as long as its limitations are considered. The findings of the existing

experimental and numerical studies showed that LTSM might be substantially deficient to predict real building responses due to its simplicity.

- The fictitious deep beam equations proposed by Burland and Wroth (1974) were re-expressed as a transfer function ($\Delta/L = C\varepsilon_{crit}$), and the interpretation of the $\Delta/L - L/H$ relationship was simplified by focusing on the coefficient 'C'. The original deep beam equations were also modified to include the effect of the average horizontal strain. Furthermore, an evaluation of the simply modified and current deep beam equations was performed using the reported data and observed damage classes of case studies available in the literature. The results showed that the observed damage and measured crack widths are more or less compatible with the limiting tensile strain boundaries. It was shown that for the cases in which moderate or higher damage was observed, the original deep beam equations tend to underestimate the resultant damage class. However, being quite conservative as a result from the direct application of free-field ground settlements, the mentioned underestimation is most probably compensated during the evaluations made by LTSM.

References

Basile, F. (2014). Effects of tunnelling on pile foundations. *Soils and Foundations, 54*, 280-295. doi:10.1016/j.sandf.2014.04.004

Bjerrum, L. (1963). *Allowable settlement of structures.* Proceedings of the 3rd European Conference on Soil Mechanics and Foundation Engineering, Wiesbaden, Germany.

Boone, S. J. (1996). Ground-movement-related building damage. *Journal of Geotechnical Engineering, 122*, 886-896. doi:10.1061/(asce)0733-9410(1996)122:11(886)

Boonpichetvong, M., Netzel, H., & Rots, J. (2006). Numerical analyses of soil-foundation-building interaction due to tunnelling. In K. J. Bakker, A. Bezuijen, W. Broere, & E. A. Kwast (Eds.), *Geotechnical aspects of underground construction in soft ground-bakker*. London: Taylor & Francis.

Boscardin, M. (1980). *Building response to excavation-induced ground movements* (Ph.D. Thesis). University of Illinois at Urbana-Champaign, Champaign, IL.

Boscardin, M. D., & Cording, E. J. (1989). Building response to excavation-induced settlement. *Journal of Geotechnical Engineering, 115*, 1-21. doi:10.1061/(asce)0733-9410(1989)115:1(1)

Burd, H. J., Houlsby, G. T., Augarde, C. E., & Liu, G. (2000). Modelling tunnelling-induced settlement of masonry buildings. *Proceedings of the Institution of Civil Engineers - Geotechnical Engineering, 143*, 17-29. doi:10.1680/geng.2000.143.1.17

Burhouse, P. (1969). Composite action between brick panel walls and their supporting beams. *Proceedings of the Institution of Civil Engineers, 43*, 175-194. doi:10.1680/iicep.1969.7381

Burland, J., Mair, R., & Standing, J. (2004). Ground performance and building response due to tunnelling. In R. J. Jardine, D. M. Potts, and K. G. Higgins (Eds.), *Advances in Geotechnical Engineering. Institution of Civil Engineers, 1*, 291-342.

Burland, J., & Wroth, C. (1974). *Settlement of buildings and associated damage.* Proceedings of conference on settlement of structures, Cambridge.

Burland, J. B. (1997). Assessment of risk of damage to buildings due to tunnelling and excavation. In K. Ishihara (Ed.), *Earthquake geotechnical engineering*. Rotterdam: Balkema.

Burland, J., Broms, B., & de Mello, V. (1977). *Behavior of foundations and structures*. 9th International Conference on Soil Mechanics and Foundation Engineering, Tokyo.

Clarke, J. A., & Laefer, D. F. (2014). Evaluation of risk assessment procedures for buildings adjacent to tunnelling works. *Tunnelling and Underground Space Technology, 40*, 333-342. doi:10.1016/j.tust.2013.10.014

Clough, G. W., & O'Rourke, T. D. (1990). Construction induced movements of in-situ walls. *Design and Performance of Earth Retaining Structures*, *ASCE, 25*, 439-470.

Comodromos, E. M., Papadopoulou, M. C., & Konstantinidis, G. K. (2014). Numerical assessment of subsidence and adjacent building movements induced by TBM-EPB tunneling. *Journal of Geotechnical and Geoenvironmental Engineering, 140*, 04014061. doi:10.1061/(asce)gt.1943-5606.0001166

Cook, D. (1994). *Studies of settlement and crack damage in old and new facades.* Proceedings of the 3rd international masonry conference, London.

Fargnoli, V., Gragnano, C. G., Boldini, D., & Amorosi, A. (2015). 3D numerical modelling of soil–structure interaction during EPB tunnelling. *Géotechnique, 65*, 23-37. doi:10.1680/geot.14.p.091

Farrell, R., Mair, R., Sciotti, A., & Pigorini, A. (2014). Building response to tunnelling. *Soils and Foundations, 54*, 269-279. doi:10.1016/j.sandf.2014.04.003

Finno, R. J., Voss, F. T., Rossow, E., & Blackburn, J. T. (2005). Evaluating damage potential in buildings affected by excavations. *Journal of Geotechnical and Geoenvironmental Engineering, 131*, 1199-1210. doi:10.1061/(asce)1090-0241(2005)131:10(1199)

Fok, P., Neo, B. H., Goh, K. H., & Wen, D. (2012). Assessing the impact of excavation-induced movements on adjacent buildings. *The IES Journal Part A: Civil & Structural Engineering, 5,* 195-203. doi:10.1080/19373260.2012.696444

Franzius, J. N., Potts, D. M., & Burland, J. B. (2006). The response of surface structures to tunnel construction. *Proceedings of the Institution of Civil Engineers - Geotechnical Engineering, 159*, 3-17. doi:10.1680/geng.2006.159.1.3

Giardina, G. (2013). *Modelling of settlement induced building damage* (Ph.D. thesis). Delft University of Technology, Delft.

Giardina, G., DeJong, M. J., & Mair, R. J. (2015b). Interaction between surface structures and tunnelling in sand: Centrifuge and computational modelling. *Tunnelling and Underground Space Technology, 50*, 465-478. doi:10.1016/j.tust.2015.07.016

Giardina, G., Hendriks, M. A. N, & Rots, J. G. (2014). Damage functions for the vulnerability assessment of masonry buildings subjected to tunneling. *Journal of Structural Engineering, 141*, 04014212.

Giardina, G., Hendriks, M. A. N., & Rots, J. G. (2015a). Sensitivity study on tunnelling induced damage to a masonry façade. *Engineering Structures, 89*, 111-129. doi:10.1016/j.engstruct.2015.01.042

Giardina, G., Marini, A., Hendriks, M. A. N., Rots, J. G., Rizzardini, F., & Giuriani, E. (2012). Experimental analysis of a masonry façade subject to tunnelling-induced settlement. *Engineering Structures, 45*, 421-434. doi:10.1016/j.engstruct.2012.06.042

Goh, K. H., & Mair, R. J. (2014). Response of framed buildings to excavation-induced movements. *Soils and Foundations, 54*, 250-268. doi:10.1016/j.sandf.2014.04.002

Hsieh, P. G., & Ou, C. Y. (1998). Shape of ground surface settlement profiles caused by excavation. *Can. Geotech. J., 35,* 1004-1017. doi:10.1139/cgj-35-6-1004

Laefer, D. F., Ceribasi, S., Long, J. H., & Cording, E. J. (2009). Predicting RC frame response to excavation-induced settlement. *Journal of Geotechnical and Geoenvironmental Engineering, 135*, 1605-1619. doi:10.1061/(asce)gt.1943-5606.0000128#sthash.U9779Lxw.dpuf

Mair, R., & Taylor, R. (2001). Elizabeth House: Settlement predictions. In J. B. Burland, J. R. Standing, & F. M. Jardine (Eds.), *Building response to tunnelling: Case studies from construction of the jubilee line extension, London*. London: Thomas Telford.

Mair, R., Taylor, R., & Burland, J. (1996). *Prediction of ground movements and assessment of risk of building damage due to bored tunnelling.* Fourth International Symposium of International Conference of Geotechnical Aspects of on Underground Construction in Soft Ground.

Meyerhof, G. G. (1956). Discussion on paper by Skempton et al. 'Settlement analysis of six structures in Chicago and London. *Proc Instn Civ Engrs, 5*, 170.

Mroueh, H., & Shahrour, I. (2002). Three-dimensional finite element analysis of the interaction between tunneling and pile foundations. *International Journal for Numerical and Analytical Methods in Geomechanics, 26*, 217-230. doi:10.1002/nag.194

Mroueh, H., & Shahrour, I. (2003). A full 3-D finite element analysis of tunneling–adjacent structures interaction. *Computers and Geotechnics, 30*, 245-253. doi:10.1016/s0266-352x(02)00047-2

Murphy, J., Gaynor, S., & Laefer, D. F. (2010). Predicted tunnel-induced settlement and damage to Findlater's Church with respect to freefield and constructed side considerations. GeoFlorida 2010 (ASCE): Advances in Analysis, Modeling & Design, Florida. doi:10.1061/41095(365)171#sthash.3LTMWsmI.dpuf

Netzel, H. (2009). *Building response due to ground movements* (Ph.D. thesis). Delft University of Technology, Delft.

Peck, R. (1969). *Deep excavations and tunneling in soft ground.* Proceedings of the 7th international conference on soil mechanics and foundation engineering, Mexico.

Polshin, D., & Tokar, R. (1957). *Maximum allowable non-uniform settlement of structures*. Proceedings of the fourth international conference on soil mechanics and foundation engineering, London.

Potts, D. M., & Addenbrooke, T. I. (1997). A structure's influence on tunnelling-induced ground movements. *Proceedings of the Institution of Civil Engineers - Geotechnical Engineering, 125*, 109-125. doi:10.1680/igeng.1997.29233

Skempton, A. W., & Macdonald, D. H. (1956). The allowable settlements of buildings. *Proceedings of the Institution of Civil Engineers, 5*, 727-768. doi:10.1680/ipeds.1956.12202

Son, M. (2003). *The response of buildings to excavation-induced ground movements* (Ph.D. dissertation). University of Illinois at Urbana-Champaign, Champaign, IL

Son, M., & Cording, E. J. (2005). Estimation of building damage due to excavation-induced ground movements. *Journal of Geotechnical and Geoenvironmental Engineering, 131*, 162-177. doi:10.1061/(asce)1090-0241(2005)131:2(162)

Son, M., & Cording, E. J. (2007). Evaluation of building stiffness for building response analysis to excavation-induced ground movements. *Journal of Geotechnical and Geoenvironmental Engineering, 133*, 995-1002. doi:10.1061/(asce)1090-0241(2007)133:8(995)

Terzaghi, K. (1935). The actual factor of safety in foundations. *Struc Eng, 13*, 126.

Timoshenko, S. (1957). *Strength of materials-Part 1 'Elementary theory and problems'.* London: D van Nostrand Co Inc.

Figure Captions

Figure 1. (a) Different positions of buildings in the transverse settlement trough: (i) sagging, (ii) at an inflection point and (iii) hogging. (b) Possible ground settlements due to deep excavations (modified from Hsieh and Ou, 1998)

Figure 2. Deformation measures for a masonry wall conforming to a ground settlement profile in (a) the sagging zone, (b) both the sagging and hogging zones and (c) the hogging zone and the typical building damages or response (d, e, f and g).

Figure 3. Fictitious deep beam model (Burland and Wroth, 1974).

Figure 4. Damage prediction diagrams of (a) Boscardin and Cording (1989) and (b) Burland (1997).

Figure 5. $C - L/H$ composite curves obtained for different values of E/G: (a) for sagging and (b) for hogging.

Figure 6. Variation of $C_b{}^*$ and $C_d{}^*$ functions with L/H.

Figure 7. Comparison between calculated decisive C values and back-calculated $C_{(low)}$-$C_{(up)}$ ranges
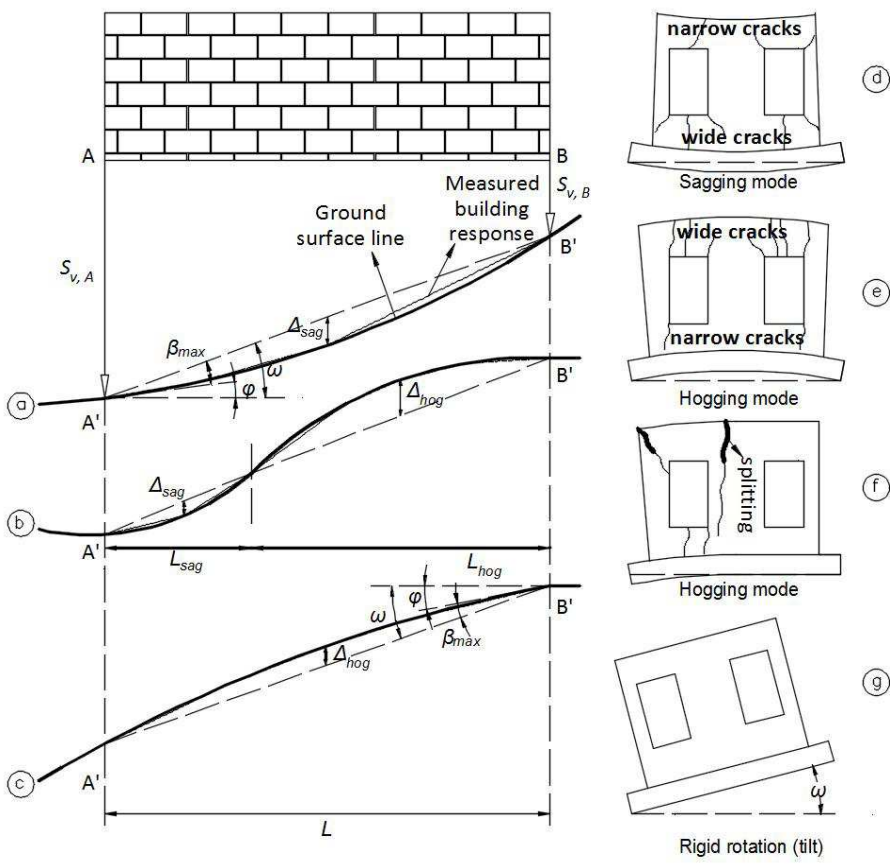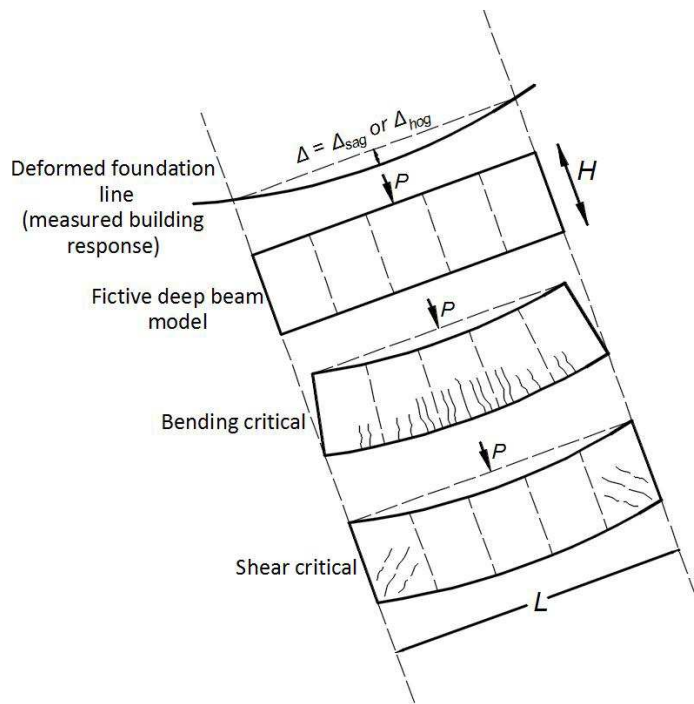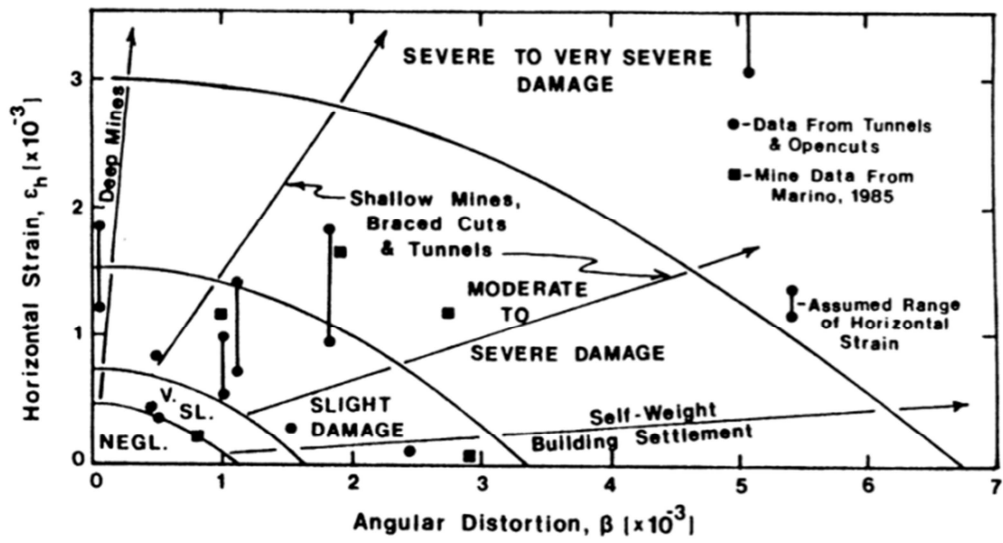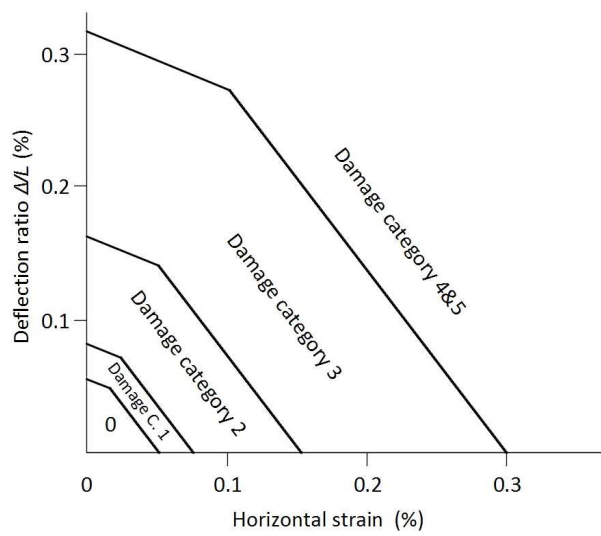
Figure 1
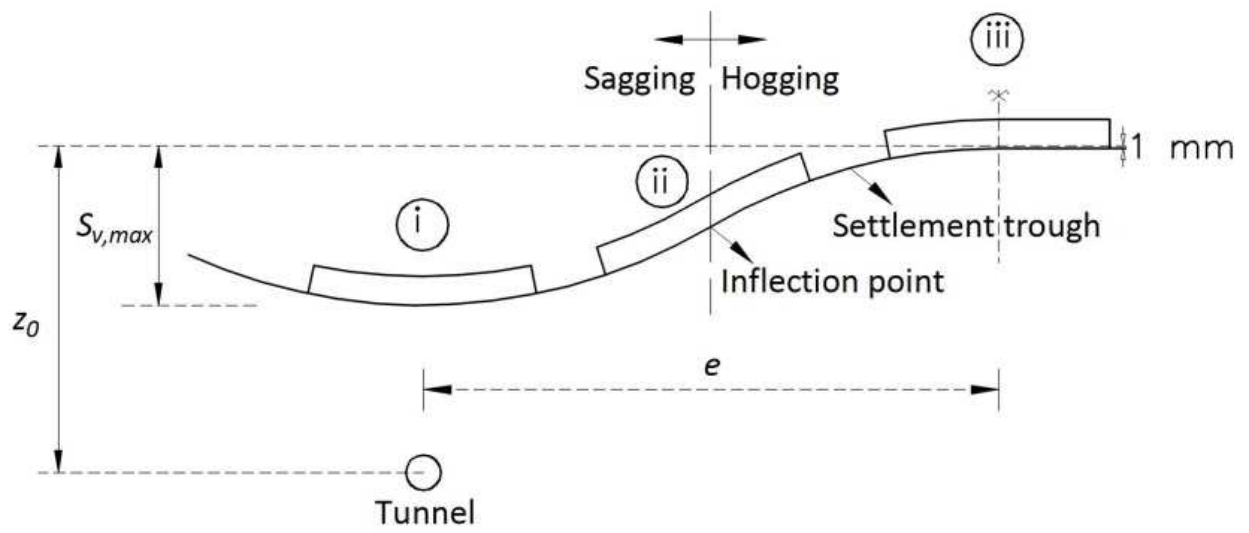
(a)
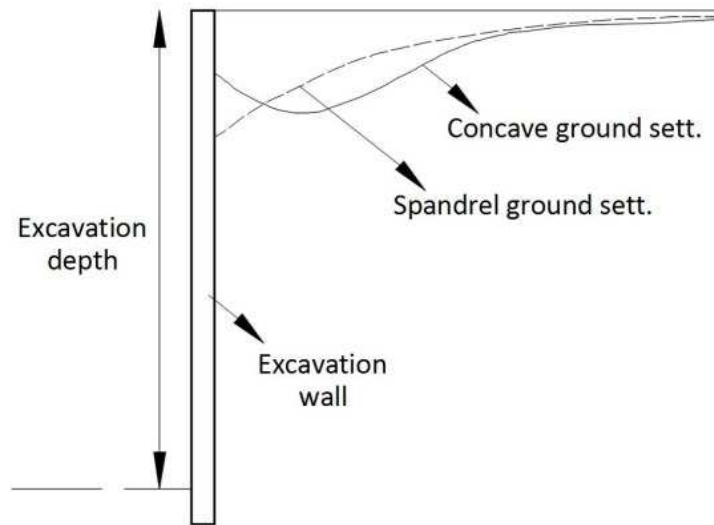
(b)

Figure 2
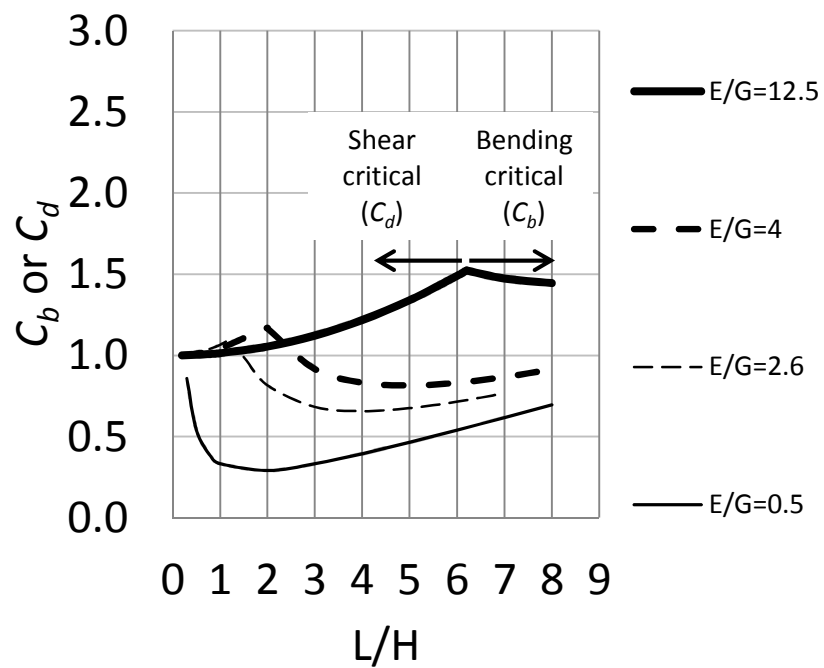
Figure 3

Figure 4

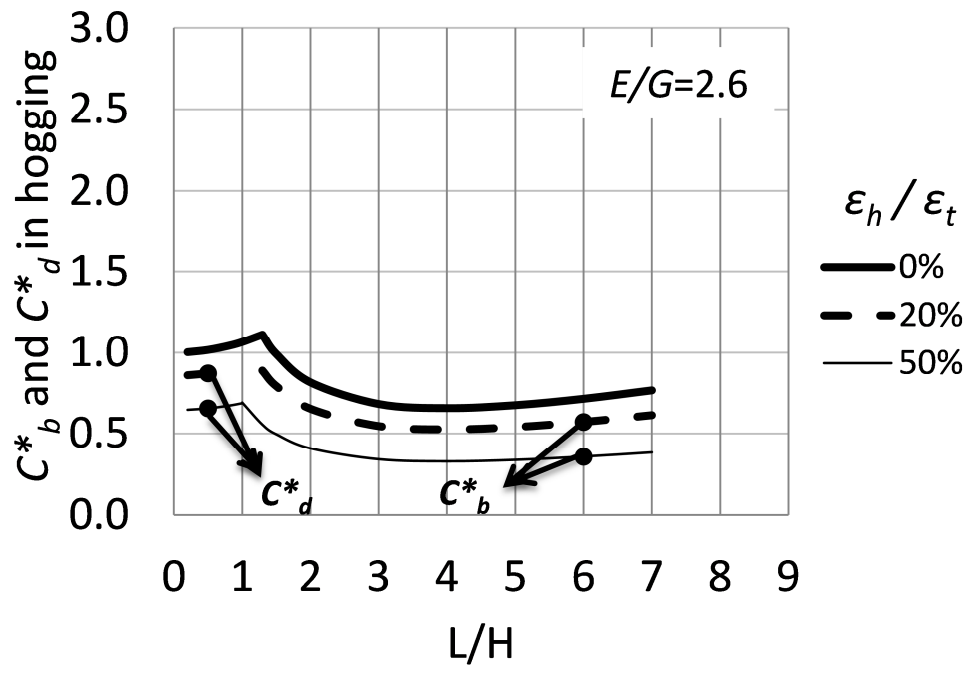
(a)

(b)

Figure 5
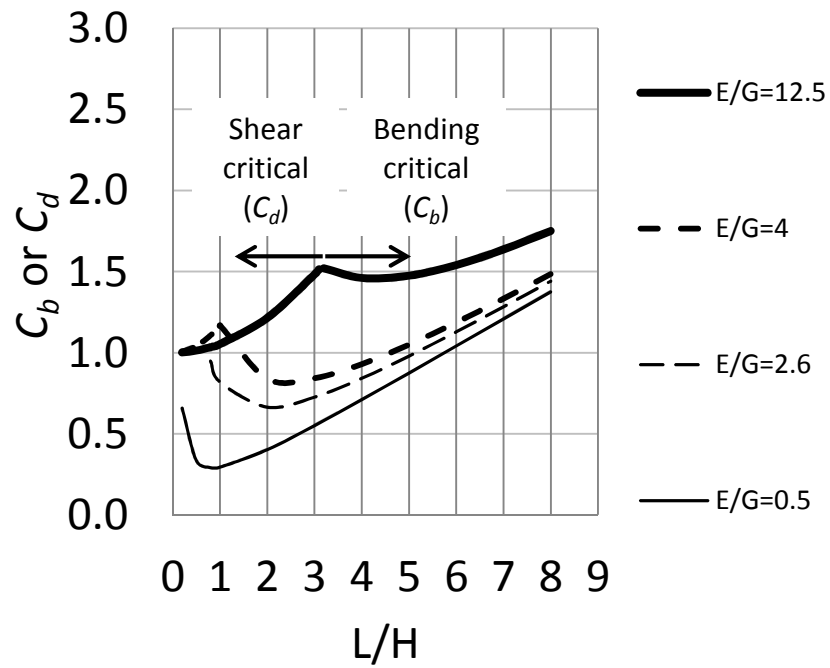
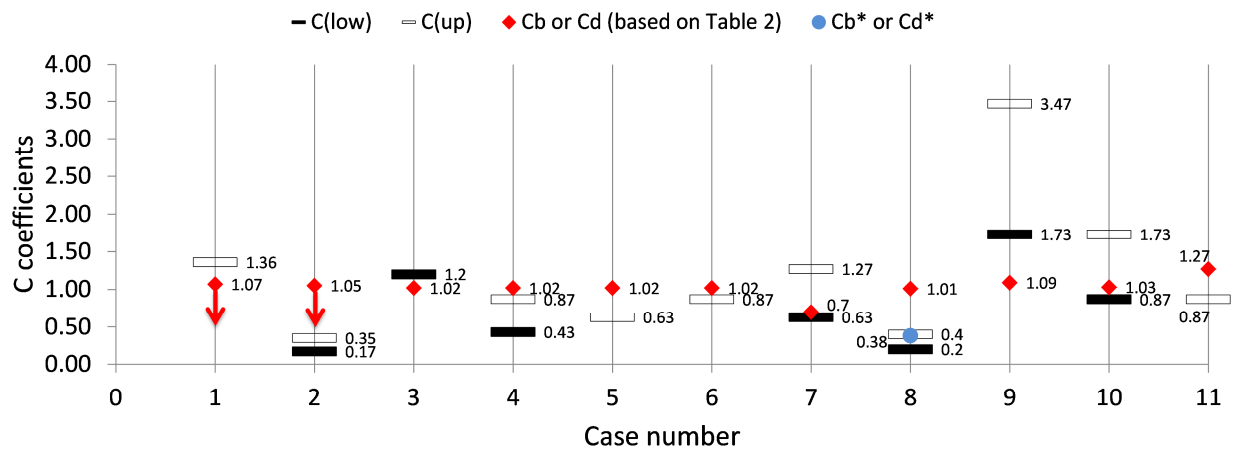(a)

(b)

Figure 6

Figure 7

Table 1. Damage classification table (modified from Burland et al., 1977 and Boscardin & Cording, 1989).

Category of damage	Damage class	Description of typical damage and ease of repair [a,b]	Approximate crack width[c] (mm)	ε_{lim} (%) After Boscardin and Cording (1989)	
				$\varepsilon_{lim(low)}$	$\varepsilon_{lim(up)}$
Aesthetic damage	0-Negligible	Hairline cracks	Up to 0.1 mm	0.000	0.050
	I-Very slight	Fine cracks that can easily be treated during normal decoration.	Up to 1 mm	0.050	0.075
	II-Slight	Cracks can be easily filled. Cracks are visible externally.	Up to 5 mm	0.075	0.150
Functional damage affecting serviceability	III-Moderate	The cracks require some opening up and can be patched by a mason.	5 to 15 mm or a number of cracks larger than 3 mm	0.150	0.300
	IV-Severe	Includes large cracks. Extensive repair work is required.	15 to 25 mm but also depends on the number of cracks	> 0.300	
Structural damage affecting stability	V-Very severe	Beams lose bearing, walls lean and require shoring, and there is a danger of structural instability.	Usually larger than 25 mm but also depends on the number of cracks	> 0.300	

Notes:
[a] Location of damage in the building or structure must be considered when classifying the degree of damage.
[b] Descriptions are shortened for brevity. Refer to Burland et al. (1977) for full descriptions.
[c] Crack width is only one aspect of damage and should not be used alone as a direct measure of it.

Table 2. The equations extracted from fictitious deep beam equations (Equations (4)-(5)) to calculate C_b and C_d coefficients.

C coefficients	Sagging ($t = H/2$)	Hogging ($t = H$)
C_b (extracted from Equation (4) for bending critical cases)	$0.17\dfrac{L}{H} + 0.25\dfrac{H}{L}\dfrac{E}{G}$	$0.083\dfrac{L}{H} + 0.5\dfrac{H}{L}\dfrac{E}{G}$
C_d (extracted from Equation (5) for shear critical cases)	$1 + 0.67\left(\dfrac{L}{H}\right)^2\dfrac{G}{E}$	$1 + 0.17\left(\dfrac{L}{H}\right)^2\dfrac{G}{E}$

Table 3. The reported features of the case studies

Case reference and number		L/H	E/G	$(\Delta/L)_{meas}$	ε_h	$\dfrac{\varepsilon_h}{0.0006}$	Damage state and max. crack width (mm) at $(\Delta/L)_{meas}$	Observed damage class $\varepsilon_{lim(low)}$ $\varepsilon_{lim(up)}$
Boscardin and Cording (1989)	1	1.00	2.60	Hogging 5.6×10^{-3}	7.5×10^{-3}	12.5	Severe diagonal cracking near to window openings	Severe (0.003, higher)
Son (2003)	2	2.00	12.9 [a]	Hogging 0.53×10^{-3}	1.7×10^{-3}	2.83	Diagonal cracks around 10 mm	Moderate (0.0015, 0.0030)
Giardina et al. (2012)	3	1.21	11.0	Hogging 6.00×10^{-4}	0	0	Hairline cracks	Negligible (0.0000, 0.0005)
	4	1.21	11.0	Hogging 1.30×10^{-3}	0	0	Many cracks from 5 to 15 mm	Moderate (0.0015, 0.0030)
	5	1.21	11.0	Hogging 1.90×10^{-3}	0	0	Many cracks from 15 to 25 mm	Severe (0.003, higher)
	6	1.21	11.0	Hogging 2.60×10^{-3}	0	0	Many cracks larger than 25 mm	Very severe (0.003, higher)
Farrell et al. (2013)	7	2.75	2.60	Sagging 1.90×10^{-3}	-0.32×10^{-3}	N/A	Cracking	Moderate (0.0015, 0.0030)
	8	0.42	2.60	Hogging 0.6×10^{-3}	0.53×10^{-3}	0.88	Severe cracking	Moderate (0.0015, 0.0030)
Giardina et al. (2014)	9	1.21	2.60	Hogging 2.60×10^{-3}	0	0	-	Slight (0.075, 0.150)
	10	1.21	8.00	Hogging 2.60×10^{-3}	0	0	-	Moderate (0.0015, 0.0030)
	11	1.21	11.0	Sagging 2.60×10^{-3}	0	N/A	-	Very severe (0.003, higher)

Note: [a] This value was extrapolated by using the opening ratio - E/G relationships given by Son and Cording (2007) for a shear/normal stiffness ratio of 1/8 for the joints.